Theofanous, M., Prospert, T., Knobloch, M. and Gardner, L. (2016). The continuous strength method for steel cross-section design at elevated temperatures. Thin-Walled Structures. **98**, 94-102.

The continuous strength method for steel cross-section design at elevated temperatures

Theofanous M.[1], Propsert T.[2], Knobloch M.[3] and Gardner L.[2]

[1] University of Birmingham, UK
[2] Department of Civil and Environmental Engineering, Imperial College London, London, SW7 2AZ, UK.
[3] University of Bochum, Germany

Corresponding author: Prof Leroy Gardner, Department of Civil and Environmental Engineering, Imperial College London, London, SW7 2AZ, UK. Email: Leroy.gardner@imperial.ac.uk

Abstract

When subjected to elevated temperatures, steel displays a reduction in both strength and stiffness, its yield plateau vanishes and its response becomes increasingly nonlinear with pronounced strain hardening. For steel sections subjected to compressive stresses, the extent to which strain hardening can be exploited (i.e. the strain at which failure occurs) depends on the susceptibility to local buckling. This is reflected in the European guidance for structural fire design EN1993-1-2 [1], which specifies different effective yield strengths for different cross-section classes. Given the continuous rounded nature of the stress-strain curve of structural steel at elevated temperatures, this approach seems overly simplistic and improved accuracy can be obtained if strain-based approaches are employed [2]. Similar observations have been previously made for structural stainless steel design at ambient temperatures and the continuous strength method (CSM) was developed as a rational means to exploit strain hardening at room temperature. This paper extends the CSM to the structural fire design of steel cross-sections. The accuracy of the method is verified by comparing the ultimate capacity predictions with test results extracted from the literature. It is shown that the CSM offers more accurate ultimate capacity predictions than current design methods throughout the full temperature range that steel structures are likely to be exposed to during a fire.

Moreover due to its strain-based nature, the proposed methodology can readily account for the effect of restrained thermal expansion on the structural response at cross-sectional level.

Keywords: Continuous strength method, Structural fire design, Elevated temperatures, Steel structures, Stub column, Cross-section resistance

1. Introduction

The behaviour and design of steel structures subjected to fire poses a great challenge for both practising engineers and researchers due to its complexity and the severe safety and economic implications. At high temperatures, steel structures experience a substantial deterioration of their material characteristics and the development of thermal strains, which are, in most cases, non-uniform both along the member length and through the cross-section, whilst creep also becomes increasingly significant. These features, coupled with the inherent uncertainty associated with fire loading, have prompted widespread research, focusing on various aspects of structural fire design.

The resistance of steel structures under fire conditions can be considered on four levels [3]: The material behaviour at elevated temperatures (Level 1); the cross-sectional behaviour considering local stability effects (Level 2); the member behaviour considering global stability effects (Level 3); and the global structural behaviour considering effects based on large deformations, change of structural systems and alternative load paths (Level 4). Experimental research on the behaviour of steel structures under fire is mainly restricted to the study of the material (Level 1) and structural response of isolated members (Level 2 and 3), due to the high cost and complexity associated with testing of full-scale structures under fire. Nonetheless some fire tests on frame sub-assemblies [4], plane frames [5] and complete structures [6] (Level 4) have been reported. Numerous isothermal tests on isolated long columns [7-9], stub columns [10] and beams [11, 12] have been conducted to investigate the effect of high temperature on the structural response of members failing by local buckling or

overall buckling without the added complexity of the effects of heating rate. Tests on isolated members [13, 14] subjected to standardized fire curves [15], which allow a more realistic representation of the structural response of members in fire, have also been performed and are utilized to obtain critical temperatures as a function of parameters such as the load level and the member slenderness [16].

Key to the structural response of either an isolated member or a complete structure subjected to elevated temperatures is the material response. Therefore, in addition to tests on structural members, numerous experimental studies have been conducted to study the effect of temperature on the material response of structural steel of various grades [17-19], cold-formed steel [20] and stainless steel [21, 22]. At elevated temperatures, the stress-strain curve of structural steel has been shown to deviate significantly from the elastic-perfectly plastic one traditionally assumed for steel design at ambient temperature [23] and becomes increasingly rounded with a pronounced loss of stiffness and strength and significant strain hardening occurring at low strains. The influence of strain rate [24] and heating rate on material response, depending on whether the experimental procedure followed is isothermal or transient, has also been studied [25]. Based on experimental results, suitable reduction factors for stiffness (i.e. Young's modulus) and strength (i.e. ultimate tensile stress, effective yield stress and various proof stresses) have been proposed for the various material grades investigated. Moreover, material models reflecting the rounded nature of the stress-strain response of steel at elevated temperatures have been developed. The model proposed by Rubert and Schaumann [26], which assumes an elliptical transition from the end of the elastic range up to the effective yield strength corresponding to 2% strain has been adopted in EN 1993-1-2 [1] and implicitly accounts for the effect of creep. Other material models, usually variants of the Ramberg-Osgood model [27, 28] and originally developed for stainless steel at ambient temperature [29-32], have also been proposed [17-22].

This paper focuses on the structural response of steel members failing by local buckling at elevated temperatures. The continuous strength method (CSM), which was originally developed as a deformation-based approach to rationally incorporate strain hardening into the design of stainless steel [32-34] and structural steel [35, 36] cross-sections at room

temperature, is extended herein to cover the design of steel sections at elevated temperatures. Existing experimental data are first reviewed in Section 2 and subsequently used for the development and validation of the CSM in Sections 3 and 4, respectively.

2. Review of existing experimental studies

Key to the development of the CSM for steel sections at elevated temperatures is the collation of relevant test data against which the method can be validated. Given the high scatter typically encountered in the results of structural fire tests and the numerous factors affecting structural response at elevated temperatures, only isothermal test results on isolated steel stub columns and beams with unrestrained thermal expansion are utilized herein for the development and assessment of the method. Tests extracted from the literature are summarized in Section 2.1, recent experiments reported by the third author and his co-workers [37] are described in Section 2.2, where the aspects of these tests relevant to the deformation-based design approach developed herein are expanded upon.

2.1 Test data extracted from the literature

The primary focus of the CSM is deformation-based design and the exploitation of strain hardening. Experimental data are therefore sought on non-slender cross-sections which exhibit material nonlinearity prior to failure. Slender (i.e. Class 4) cross-sections are not currently covered by the CSM and can be designed using the traditional effective width method [1, 38]. Hence experimental studies on slender steel sections at elevated temperatures have not been considered herein.

A total of 42 isothermal test results on concentrically loaded non-slender stub columns have been gathered and are summarized in Table 1. The tested sections include SHS and I-sections of various slendernesses, while the material grades covered include hot-rolled structural steel [7, 9] and fire resistant steel [10]. Excluding the tests performed at room temperature and

those where insufficient information was provided for the elevated temperature material properties, left 26 test results from the literature suitable for the development of the CSM. These test data were augmented with the results of a series of tests recently performed at ETH Zurich [37], for which the material properties are reported in detail in [24]; these tests are summarised in the Section 2.2. All collated experimental results are utilized in Section 3 to develop and assess the CSM for steel sections at elevated temperatures.

2.2 Additional recent test data from ETH Zurich

The experimental data collected from the literature are supplemented with the results of additional tests recently performed at ETH Zurich [37], which are outlined herein, with the key aspects relevant to the development of the CSM expanded upon. The testing programme comprised a total of 106 structural tests at elevated temperatures (stub and slender column tests loaded concentrically and eccentrically) as well as corresponding material coupon tests at various temperatures and strain rates. SHS and RHS (square and rectangular hollow sections), as well as HEA sections, were examined. Given the high sensitivity of the material response to strain rate at elevated temperatures [24], only specimens for which the material response was obtained at a strain rate matching the strain rate of the stub column tests have been included in the subsequent analysis.

Steady state tensile material coupon tests were carried out to determine the elevated temperature material behaviour of the steel sections used for the stub column tests. An electric furnace with three vertically distributed heating zones was used for the elevated temperature tests. In addition to the overall stress-strain relationship, the mechanical parameters, including the modulus of elasticity, the proportional limit, the 0.2% proof stress and effective yield strengths at different levels of total strain, were obtained from the test results. Fig. 1 shows the stress-strain relationships at different temperatures obtained from tensile coupons taken from the stub column specimens and tested at a strain rate of 0.10 %/min as an example. Details of the test setup and results are given in [24].

A series of steady state stub column tests at ambient and elevated temperatures under uniform axial compression was performed to determine their cross-sectional capacity. Measurements of the geometry of the specimens were taken prior to testing and are summarised in Table 2. Initial geometric imperfection measurements were made using a three-dimensional video extensometer, utilising two cameras. Fig. 2 shows the stub column testing arrangement which consists of the following main parts: an electric furnace with four vertically distributed heating zones, a double-action hydraulic loading jack with a capacity of 4.45 MN and a reaction frame.

Full axial load-end shortening histories were recorded, including the post-ultimate range. The relative vertical displacement, i.e. the end shortening of the stub columns, was determined using two LVDTs located beneath the furnace. The LVDTs recorded the relative vertical displacement between the mid-heights of the 80 mm thick parallel end-plates of the testing device using two stainless steel bars. The axial load was measured using four load cells placed above the upper piston and outside the furnace. The vertical load was calculated as the sum of the measured vertical loads of the four cells. Three thermocouples were used to measure the temperature at the top, bottom and mid-height of one stub column surface.

Applying the steady state testing method, the specimens were first uniformly heated with a heating rate of 5 °C/min (furnace air temperature) to the target temperatures of 400 °C, 550 °C and 700 °C. During heating, a constant axial compressive load of approximately 5 kN was applied to the specimens. The thermal elongation during heating was not restrained. After reaching the target temperature, closed-loop strain-controlled (via the LVDTs) compressive loading was applied at strain rates of 0.1 %/min, 0.02 %/min and 0.01 %/min. More information about the test setup and measurements is given in [39].

Fig. 3 shows the axial load-end shortening curves of the SHS (top), RHS (middle) and HEA (bottom) test specimens with a strain rate of 0.1 %/min at 550 °C as examples. The ultimate loads N_u and the end shortening at ultimate load δ_u are given in Table 2. The resistance at 400 °C, 550 °C and 700 °C was reduced to 65 %, 38 % and 11 % of the resistance at room temperature for the SHS specimens, to 84 %, 53 % and 15 % for the RHS specimens and to

89 %, 45 % and 14 % for the HEA specimens. Further details of the test results are given in [39].

3. Deformation based design for steel structures at elevated temperatures

3.1 Response of steel plates and sections at elevated temperatures

The dependence of failure stress on cross-section slenderness of compressed sections is reflected in EN 1993-1-2 [1], which specifies different effective yield strength values according to the susceptibility of a cross-section to local buckling, as assessed on the basis of cross-section classification. Due to the discrete nature of classification, a step in the structural capacity occurs between slender and non-slender sections, as two distinct levels of effective stress are specified. Moreover, the utilization of the elastic section modulus for Class 3 sections and the plastic section modulus for Class 1 and 2 sections induces a second step in the capacity of steel beams at elevated temperatures. In reality the cross-section resistance decreases continuously with increasing cross-section slenderness and any discontinuities occurring at the transition between the various classes are due to the stress-based approach underlying the cross-section classification process. The absence of a sharply defined yield stress renders the cross-section classification process, commonly employed for the design of metallic structures at both room and elevated temperature [1, 29], unrepresentative of the actual response, since no specific stress value exists at which a sudden loss of stiffness occurs and increasing strain is generally accompanied by hardening of the material.

Knobloch and Fontana [2] recognised the shortcomings associated with a stress based method in the absence of a sharply defined yield stress and found that the design provisions in EN 1993-1-2 [1] overestimate the resistance of stocky (Class 1-2) plates at room temperature and underestimate the resistance of slender (Class 4) plates at elevated temperatures [2]. A modified Winter formula was proposed to reduce the strength for the complete range of slenderness values. Unlike the effective width method used in Eurocode 3, which is based on an elastic stress distribution for both ambient and elevated temperatures, the strain-based

approach proposed in [2] uses a plastic stress distribution. The main advantages of the method proposed in [2] stem from its strain-based nature and include the avoidance of cross-section classification, the consideration of the non-linear material behaviour of carbon steel at elevated temperatures and the more realistic representation of the actual structural response. However, the extension of the effective width method across the full slenderness range renders this method rather laborious. A further shortcoming of the approach [2], which is in common with the current EN 1993-1-2 treatment, is the consideration of individual plate behaviour, rather than that of the full cross-section. This disregards any interaction between the constituent plate elements of a section and, in the context of [2], means that the ultimate strength of the individual plates is reached at different strains and thus also at different load levels. In practice, compatibility dictates common strains at the intersections of connecting plates, which should be reflected in the design approach. Finally, improvements to the material model adopted in [2] to capture better the strain hardening response of steel at elevated temperatures, may be achieved. Both the effect of strain hardening and element interaction are accounted for by the continuous strength method, which is a strain-based design approach, extended to steel elements in fire herein.

3.2 Background to the CSM

The continuous strength method (CSM) was originally developed [32-36] as a design approach which rationally exploits the significant strain hardening exhibited by stocky stainless steel cross-sections under load. The main principle underlying the method is that the exploitation of strain hardening for cross-sections subjected to compressive stresses is limited by the occurrence of local buckling. On this basis, an empirical relationship, referred to as the 'base curve', between the level of strain that a given cross-section can attain prior to failure by local buckling and cross-section slenderness, was developed. Element interaction is accounted for [33] by utilizing the cross-section slenderness, rather than simply considering the most slender individual plate element. The method has also been extended to cover structural steel [35, 36] and aluminium [40, 41] design at room temperature.

There is an analogy between the response of stainless steel structures and that of steel structures at elevated temperatures [2], since in both cases the material displays no yield plateau and exhibits pronounced strain hardening with increasing stresses. The strain that can be attained by a steel section subjected to compressive stresses prior to failure depends on its susceptibility to local buckling [9]. Stocky steel sections subjected to compressive stresses can attain high strains prior to the occurrence of local buckling and hence benefit significantly from strain hardening, whilst more slender cross-sections fail at lower strains and will not experience strain hardening. This is the case both at ambient and high temperatures. Based on the test data summarized in Section 2, the CSM is extended to cover the design of steel cross-sections at elevated temperatures. In accordance with the CSM for room temperature, the main features of the CSM for elevated temperatures are the base curve and the material stress-strain model, taking due account of the temperature effects, as discussed hereafter.

3.3 Base curve

The first step towards extending the CSM to the design of steel sections at elevated temperatures is the determination of a suitable base curve, which is in essence an empirical equation relating the cross-section deformation capacity to the cross-section slenderness. The cross-section slenderness $\bar{\lambda}_{p,\theta}$ is defined according to Eq.(1):

$$\bar{\lambda}_{p,\theta} = \sqrt{\frac{f_{0.2,\theta}}{f_{cr,\theta}}} \tag{1}$$

where $f_{0.2,\theta}$ is the 0.2% proof strength at temperature θ and $f_{cr,\theta}$ is the elastic critical local buckling stress of the cross-section, taking into account the relevant Young's modulus value E_θ at temperature θ. The elastic critical local buckling stress $f_{cr,\theta}$ of the cross-section can be obtained analytically [42] or numerically (using bespoke software such as CUFSM [43] or more general software packages), but may also be taken conservatively as that of the most slender plate element in the cross-section (i.e. ignoring element interaction).

The experimental deformation capacities were obtained directly from the load-deformation curves of the stub column tests considered, and used, in a similar manner as at room temperature [33-36], to underpin the establishment of the base curve. For stub columns failing beyond their theoretical squash load N_y, the cross-section deformation capacity $\varepsilon_{csm,\theta}$ at temperature θ is expressed in terms of the strain at failure ε_{lb} (minus 0.2% strain to ensure compatibility with the CSM material model described later), normalized by the yield strain $\varepsilon_{y,\theta}=f_{0.2,\theta}/E_\theta$ as defined in Eq.(2), whereas for stub columns failing below their squash load or beyond the yield slenderness limit of $\bar{\lambda}_{p,\theta}=0.68$ [34], the deformation capacity is obtained from Eq.(3).

$$\frac{\varepsilon_{csm,\theta}}{\varepsilon_{y,\theta}}=\frac{\varepsilon_{lb}-0.002}{\varepsilon_{y,\theta}}=\frac{\frac{\delta_u}{L}-0.002}{\varepsilon_{y,\theta}}, \quad \text{for } N_u \geq N_y \tag{2}$$

$$\frac{\varepsilon_{csm,\theta}}{\varepsilon_{y,\theta}}=\frac{N_u}{N_y}, \qquad \text{for } N_u<N_y \text{ or } \bar{\lambda}_{p,\theta}>0.68 \tag{3}$$

where ε_{lb} is the local buckling strain at failure determined as the end-shortening δ_u corresponding to the ultimate load N_u normalized by the stub column length L. Since both the cross-section slenderness and the elastic strain corresponding to $f_{0.2}$ are temperature dependant, accurate material properties at the temperature at which the stub column tests were conducted, are required for the derivation of the base curve.

On the basis of the test data summarized in Tables 1 and 2 and the material properties extracted from the relevant publications [7-10, 37], the cross-sectional slenderness values were determined according to Eq.(1) and plotted against their corresponding deformation capacities in Fig. 4. The CSM base curve applicable to both carbon steel and stainless steel at room temperatures, which is defined by Eq.(4), is also depicted.

$$\frac{\varepsilon_{csm,\theta}}{\varepsilon_{y,\theta}}=\frac{0.25}{\bar{\lambda}_{p,\theta}^{3.6}} \quad \text{but} \frac{\varepsilon_{csm,\theta}}{\varepsilon_{y,\theta}} \leq \min\left(15, \frac{0.03}{\varepsilon_{y,\theta}}\right) \quad \text{for } \bar{\lambda}_{p,\theta} \leq 0.68 \tag{4}$$

where the limiting value of 15 is to avoid excessive deformations [32-36] and the 3% strain limit is to avoid significant over-predictions of strength (not greater than 5%) from the simplified material model described in Section 3.4. Note that the 3% strain limit enables the use of strengths higher than those allowed in EN 1993-1-2, where the strength at 2% strain is employed for stocky cross-sections. The slenderness limit of 0.68 marks the transition from stocky to slender sections, beyond which, there is no benefit from strain hardening. Application of the CSM is currently limited to $\bar{\lambda}_{p,\theta} \leq 0.68$.

In Fig. 4 it can be observed that the base curve derived for carbon and stainless steel sections at room temperature provides a good, generally lower-bound fit to the results considered herein. The same data are depicted in Fig. 5, where the test results are classified according to the temperature at which they were conducted. No significant difference appears between the individual datasets. The fit is considered to be acceptable because: (1) it captures well the general trend of the test data, (2) data on deformation capacity is inherently scattered, particularly in fire, due to the relatively 'flat' nature of the regions of the load-deformation curves from which they are determined and (3) resistance predictions in the inelastic range are not overly sensitive to the precise value of deformation capacity since the strain hardening modulus is substantially lower than the initial elastic modulus of the material. Hence the base curve for the CSM at room temperature is adopted herein as the base curve for the CSM at elevated temperatures.

3.4 Material model

The selection of an appropriate material model is key to the successful extension of the CSM to steel sections at elevated temperatures. As discussed in the introductory section of this paper, various material models based on the analysis of experimental data have been proposed, the most commonly utilized being the Rubert-Schaumann model [26] adopted in EN 1993-1-2 [1] and variants of the Ramberg-Osgood model [27-31], which have been shown to provide excellent fit to the test data in a number of experimental studies [17-22]. However, the adoption of a compound Ramberg-Osgood model results in lengthy design

expressions, particularly for sections subjected to a strain gradient (i.e. bending) [36]. This complicates the design process and discourages designers from using advanced design approaches such as the CSM. Given the inherently high uncertainty associated with fire loading, a trade-off between accuracy and simplicity in the material model is sought. The adopted material model has to reflect the basic features of the actual response, whilst at the same time being sufficiently simple to facilitate design using explicit design equations rather than resorting to cumbersome numerical integration, iterative schemes or design tables.

In accordance with the latest developments of the CSM for stainless steel at ambient temperatures [34], a bilinear material model is adopted herein, which is shown to accurately capture basic material characteristics and results in efficient and accurate design. The proposed material model is defined by Eq.(5) and depicted in Fig.6. It is a function of only 3 temperature dependant material parameters readily available to the designer, namely the Young's modulus E_θ, the 0.2% proof stress $f_{0.2,\theta}$ and the 'effective yield strength' $f_{2.0,\theta}$ which is the stress value corresponding to 2% total strain at temperature θ.

$$\begin{aligned} f_{csm,\theta} &= E_\theta \, \varepsilon_{csm,\theta} && \text{for } \varepsilon_{csm,\theta} \le \varepsilon_{y,\theta} \\ f_{csm,\theta} &= f_{0.2,\theta} + E_{sh,\theta}\left(\varepsilon_{csm,\theta} - \varepsilon_{y,\theta}\right) && \text{for } \varepsilon_{csm,\theta} > \varepsilon_{y,\theta} \end{aligned} \tag{5}$$

where $E_{sh,\theta}$ is the strain hardening slope at temperature θ, given by:

$$E_{sh,\theta} = \frac{f_{2.0,\theta} - f_{0.2,\theta}}{0.02 - \varepsilon_{y,\theta}} \tag{6}$$

In addition to the mathematical formulation of the material model, account need be taken of the effect of temperature on the basic model parameters. Clearly the determination of accurate temperature dependant material parameters is crucial for the successful application of the CSM. Although measured values for these key properties are used for the comparisons shown herein, it is proposed that the reduction factors given in EN1993-1-2 [1], which have been underpinned by extensive material testing, are used by designers when applying the CSM.

3.5 Cross-section resistance

For the determination of the compressive resistance of a cross-section, the strain at failure $\varepsilon_{csm,\theta}$ has to be obtained from Eq. (4) as a function of the cross-sectional slenderness. Thereafter the corresponding stress $f_{csm,\theta}$ is obtained from the bilinear elastic-linear hardening material model defined by Eq. (5), which is multiplied by the gross cross-section area A to yield the compressive resistance of the cross-section $N_{csm,\theta}$. The process is straightforward and does not require the calculation of effective properties.

For the determination of the bending resistance of a cross-section, a similar procedure is followed. Assuming a linear strain distribution through the depth of the cross-section, the maximum attainable compressive strain at failure $\varepsilon_{csm,\theta}$ is obtained from Eq. (4), which can be transformed into the corresponding stress distribution on the basis of Eq. (5). The obtained stress distribution can yield the ultimate moment resistance M_{csm} via numerical integration. In order to eliminate the need for numerical integration, a simplified though very accurate approximation for the bending resistance of RHS, SHS and I-sections, which is in line with the above assumptions has been derived [36]. For the bending resistance of cross-sections at elevated temperatures $M_{csm,\theta}$, the derived expression, given by Eq. (7) [36] can again be used to explicitly obtain the moment resistance as a function of the local buckling strain $\varepsilon_{csm,\theta}$.

$$\frac{M_{csm,\theta}}{M_{pl,\theta}} = 1 + \frac{E_{sh,\theta}}{E_{\theta}} \frac{W_{el}}{W_{pl}} \left(\frac{\varepsilon_{csm,\theta}}{\varepsilon_{y,\theta}} - 1 \right) - \left(1 - \frac{W_{el}}{W_{pl}} \right) \left(\frac{\varepsilon_{csm,\theta}}{\varepsilon_{y,\theta}} \right)^{-\alpha} \tag{7}$$

where α is a coefficient equal to 2 for RHS, SHS and I-sections bent about their major axis, and 1.2 for I-sections bent about their minor axis.

4. Validation and discussion

4.1 Assessment of CSM for stub columns at elevated temperatures

The stub column tests summarized in Tables 1 and 2 are utilized to assess the accuracy of the predictions of the CSM. For comparison purposes the conventional design approach of EN1993-1-2 [1] is also assessed. For both the Eurocode method and the CSM, the material

properties utilized in the predicted capacities $N_{u,pred}$ are the ones extracted from the tests and all partial safety factors have been set to unity. The accuracy of the predictions of each method is shown in Table 3, where the average ratios of predicted-to-experimental failure loads for each set of results, together with the corresponding coefficient of variation COV are given, where N_{EC3} and N_{csm} are the predicted compression capacities according to EN 1993-1-2 and the CSM and N_u is the ultimate test load. It can be seen that the CSM displays improved consistency of predictions (i.e. lower COV), compared to the Eurocode method, though it is slightly more conservative. The same conclusions can be drawn from Fig.7, where the CSM predictions are shown to be within a narrower band than the respective Eurocode predictions.

4.2 Assessment of CSM for cross-sections in bending at elevated temperatures

For the validation of the CSM for predicting cross-section bending resistances at elevated temperatures, isothermal test data on laterally restrained beams would ideally be utilized. However, the only relevant test data are described in [11], but the material properties at elevated temperatures are not reported. Therefore, the results of a comprehensive FE parametric study reported in [39] are utilized herein to assess the suitability of the CSM for the design of laterally restrained beams at elevated temperatures. The simulated sections include SHS, RHS and I-sections bent about both principal axes, whilst the temperatures considered vary from room temperature to 700 ˚C. The basic parameters (cross-section geometry, temperature, local slenderness range) considered in the parametric study are summarized in Table 4. From a total of 220 modelled sections, 86 have a cross-section slenderness $\bar{\lambda}_{p,\theta} \leq 0.68$ and are hence utilized for the validation of the CSM.

The numerically obtained ultimate moments M_u have been normalized by the respective plastic moment resistance ($M_{pl,\theta}=W_{pl}f_{2.0,\theta}$) and are plotted against the slenderness $\bar{\lambda}_{p,\theta}$ in Fig. 8. The data have been classified into 3 groups: I-sections bent about their major axis, I-sections bent about their minor axis and SHS and RHS bent about either axis. All sections display a reduction in strength with increasing slenderness. However, the I-sections bent about their minor axis seem to retain their strength at higher slendernesses more effectively

than the other section types. Similar observations have been made previously by Bambach et al [44], who studied the stress distributions that developed in slender I-sections bent about the minor axis at room temperature and concluded that they display significant inelastic behaviour in the attainment of the ultimate moment.

Figs. 9-11 depict the moment resistance predicted by the CSM normalized by the respective numerical ultimate moment M_u against the slenderness $\bar{\lambda}_{p,\theta}$ for I-sections under major axis bending, I-sections under minor axis bending and SHS and RHS respectively. The EN 1993-1-2 [1] predictions are also depicted, and M_{pred} is used to denote the predicted moment capacity. To facilitate the comparison of the two methods, the same data have been used for the assessment of both EN 1993-1-2 [1] and the CSM.

As shown in Fig. 9, the I-sections under major axis bending seem to be very well predicted by the CSM, whilst an increasing conservatism with increasing slenderness is displayed by the EN 1993-1-2. The predictions of both methods lie within a narrow band. On the other hand, the capacity of I-sections subjected to minor axis bending seems to be significantly under-predicted by both methods, as evidenced in Fig. 10. The EN 1993-1-2 approach appears to be consistently highly conservative, with the degree of conservatism increasing with increasing slenderness, whilst the conservatism is less pronounced in the CSM predictions. The high conservatism exhibited by the EN1993-1-2 predictions is believed to relate to the inability of the design method to account accurately for the actual inelastic stress distribution exhibited by slender I-sections in minor axis bending at room temperatures [44]. Moreover, the large 'step' displayed by the EN 1993-1-2 predictions occurs at the Class 3 limit and relates to the high shape factor (W_{pl}/W_{el}=1.5) of the I-sections bent about their minor axis.

In Fig. 11, EN 1993-1-2 displays a wider scatter than the CSM for the prediction SHS and RHS moment resistances. Again the observed step in predicted resistances is related to the nature of the cross-section classification system, which specifies a sharp reduction in the section modulus at a discrete slenderness (i.e. Class 2) limit, whilst the continuous nature of the CSM approach eliminates such irregularities. The relative accuracy of both methods is

quantified in Table 5 (in which M_{EC3} and M_{csm} are the moment capacities predicted by EN 1993-1-2 and the CSM), where the CSM is shown to offer clearly improved ultimate capacity predictions both in terms of consistency and design efficiency compared to the EN 1993-1-2 approach.

5. Conclusions

In fire, steel exhibits a distinctly rounded material stress-strain response with significant strain hardening occurring from low stress levels. In this paper, the continuous strength method (CSM), originally developed to incorporate the effect of strain hardening into the design of stainless steel structures at room temperature, has been extended to the design of steel cross-sections under fire. Utilising existing test data, a clear relationship between cross-section slenderness and deformation capacity was identified and an empirical equation, referred to as the base curve derived. This equation is the same as that used for stainless steel design at ambient temperatures [34]. Whilst the base curve is the same, the cross-section slenderness and the adopted strain hardening material model are different to those used for room temperature design, and reflect the elevated temperature material properties of structural steel.

The proposed CSM design approach has been validated herein against test and FE results on isolated members subjected to uniform elevated temperatures. The comparisons generally reveal that the CSM offers improved accuracy compared to the stress-based design approach set out in EN1993-1-2 [1], whilst also eliminating the artificial steps in design resistance brought about by cross-section classification. The method is, in principle, applicable to any metallic material in fire, provided that accurate material models for elevated temperatures are available. Moreover, due to its strain-based nature, the CSM can readily accommodate the effects of restrained thermal expansion, by deducting the thermal strains from the deformation capacity, within the framework of the method. Further research is underway to extend the applicability of the method to cross-sections subjected to thermal gradients, which commonly arise in practice.

Acknowledgements

The contributions of Mr Tarun Kumar Sharma and Mrs Nadiah Saari in the collation of the experimental data and their involvement in related research are gratefully acknowledged.

References

[1] EN 1993-1-2 (2005). Eurocode 3: Design of steel structures - Part 1-2: General rules - Structural fire design.

[2] Knobloch, M. and Fontana, M. (2006). Strain-based approach to local buckling of steel sections subjected to fire. Journal of Constructional Steel Research 62(1-2), 44-67.

[3] Knobloch, M. and Fontana, M. (2014). Stability of steel structures in fire - State-of-the-art, recent studies in Switzerland and future trends. Stahlbau 83(4), 257-264.

[4] Wang, Y.C. and Davies, J.M. (2003). Fire tests of non-sway loaded and rotationally restrained steel column assemblies. Journal of Constructional Steel Research 59 (3), 359-383.

[5] Rubert, A. and Schaumann, P. (1986). Structural steel and plane frame assemblies under fire action. Fire Safety Journal 10(3), 173-184.

[6] Wald, F., Simoes da Silva, L., Moore, D.B., Lennon, T., Chlanda, M., Santiago, A., Benes, M. and Borges, L. (2006). Experimental behaviour of a steel structure under natural fire. Fire Safety Journal 41 (7), 509-522.

[7] Yang, K.-C., Lee, H.-H. and Chan, O. (2006). Performance of steel H columns loaded under uniform temperature. Journal of Constructional Steel Research 62(3), 262-270.

[8] Yang, K.-C., Lee, H.-H. and Chan, O. (2006). Experimental study of fire-resistant steel H-columns at elevated temperature. Journal of Constructional Steel Research 62(6), 544-553.

[9] Yang, K.-C. and Hsu, R. (2009). Structural behavior of centrally loaded steel columns at elevated temperature. Journal of Constructional Steel Research 65(10-11), 2062-2068.

[10] Yang, K.-C., Chen, S.-J., Lin, C.-C. and Lee, H.-H. (2005). Experimental study on local

buckling of fire-resisting steel columns under fire load. Journal of Constructional Steel Research 61(4), 553-565.

[11] Vila Real, P.M.M., Piloto, P.A.G. and Franssen, J.-M. (2003). A new proposal of a simple model for lateral-torsional buckling of unrestrained steel I-beams in case of fire: experimental and numerical validation. Journal of Constructional Steel Research 59(2), 179-199.

[12] Dharma, R.B. and Tan, K.-H. (2007). Rotational capacity of steel I-beams under fire conditions. Part I: Experimental study. Engineering Structures 29 (9), 2391-2402.

[13] Mesquita, L.M.R., Piloto, P.A.G., Vaz, M.A.P. and Vila Real, P.M.M. (2005). Experimental and numerical research on the critical temperature of laterally unrestrained steel I beams. Journal of Constructional Steel Research 61(10), 1435-1446.

[14] Romero, M.L., Molinear, V., Espinos, A., Ibanez, C. and Hospitaler, A. (2011). Fire behavior of axially loaded slender high strength concrete filled tubular columns. Journal of Constructional Steel Research 67(12), 1953-1965.

[15] EN 1991-1-2 (2002). Eurocode 1: Actions on structures – Part 1-2: General actions – Actions on structures exposed to fire.

[16] Rubert, A. and Schaumann, P. (1988). Critical temperatures of steel columns exposed to fire. Fire Safety Journal 13(1), 39-44.

[17] Outinen, J., Kesti, J. and Makelainen, P. (1997). Fire design model for structural steel S355 based upon transient state tensile test results. Journal of Constructional Steel Research 42(3), 161-169.

[18] Makelainen, P., Outinen, J. and Kesti, J. (1998). Fire design model for structural steel S420M based upon transient state tensile test results. Journal of Constructional Steel Research 48(1), 47-57.

[19] Qiang, X., Bijlaard, F. and Kolstein, H. (2012). Dependence of mechanical properties of high strength steel S690 on elevated temperatures. Construction and Building Materials 30, 73-79.

[20] Chen, J. and Young, B. (2007). Experimental investigation of cold-formed steel material at elevated temperatures. Thin-Walled Structures 45(1), 96-110.

[21] Chen, J. and Young, B. (2006). Stress-strain curves for stainless steel at elevated temperatures. Engineering Structures 28(2), 229-239.

[22] Gardner, L., Insausti, A., Ng, K.T. and Ashraf, M. (2010). Elevated temperature material

properties of stainless steel alloys. Journal of Constructional Steel Research 66(5), 634-647.

[23] EN 1993-1-1. (2005) Eurocode 3: Design of steel structures - Part 1.1: General rules – General rules and rules for buildings. CEN.

[24] Knobloch, M., Pauli, J. and Fontana, M. (2013). Influence of the strain-rate on the mechanical properties of mild carbon steel at elevated temperatures. Materials and Design 49, 553-565.

[25] Anderberg, Y. (1988). Modelling steel behaviour. Fire Safety Journal 13(1), 17-26.

[26] Rubert, A. and Schaumann, P. (1985). Temperaturabhangige Werkstoffeigenschaften von Baustahl bei Brandbeanspruchung. Stahlbau 84(3), 81-86.

[27] Ramberg, W. and Osgood, W.R. (1943). Description of stress-strain curves by three parameters. Technical note No 902, Washington DC: National advisory committee for aeronautics.

[28] Hill, H.N. Determination of stress-strain relations from offset yield strength values. Technical note No 927, Washington DC: National advisory committee for aeronautics.

[29] Mirambell, E. and Real, E. (2000). On the calculation of deflections in structural stainless steel beams: an experimental and numerical investigation. Journal of Constructional Steel Research 54(1), 109-133.

[30] Rasmussen, K.J.R. 2003. Full-range stress-strain curves for stainless steel alloys. Journal of Constructional Steel Research 59(1): 47-61.

[31] Gardner, L. and Nethercot, D.A. (2004). Experiments on stainless steel hollow sections - Part 1: Material and cross-sectional behaviour. Journal of Constructional Steel Research, 60(9), 1291-1318.

[32] Gardner, L. and Theofanous, M. (2008). Discrete and continuous treatment of local buckling in stainless steel elements. Journal of Constructional Steel Research 64 (11), 1207-1216.

[33] Theofanous, M. and Gardner, L. 2012. Effect of element interaction and material nonlinearity on the ultimate capacity of stainless steel cross-sections. Steel and Composite Structures 12(1): 73-92.

[34] Afshan, S. and Gardner, L. (2013). The continuous strength method for structural stainless steel design. Thin-walled structures 68(1), 42-49.

[35] Gardner, L. (2008). The Continuous Strength Method. Proceedings of the Institution of Civil Engineers - Structures and Buildings. 161(3), 127-133.

[36] Gardner, L., Wang, F. and Liew, A. (2011). Influence of strain hardening on the behavior and design of steel structures. International Journal of Structural Stability and Dynamics. 11(5), 855-875.

[37] Pauli, J., Somaini, D., Knobloch, M. and Fontana, M. (2012). Experiments on steel columns under fire conditions. ETH Zurich, Institute of Structural Engineering. IBK Test report No. 340.

[38] Winter, G. (1947). Strength of thin steel compression flanges. Cornell University Engineering Experiment Station Bulletin No. 35/3, Ithaca, N.Y.

[39] Pauli, J. (2012). The Behaviour of Steel Columns in Fire: Material – Cross-sectional Capacity – Column Buckling. ETH Zurich, Institute of Structural Engineering. IBK report No. 343.

[40] Su, M., Young, B. and Gardner, L. (2014). Testing and design of aluminium alloy cross-sections in compression. J Struct Eng, ASCE 140 (9),

[41] Su, M., Young, B. and Gardner, L. (2014). Deformation-based design of aluminium alloy beams. Engineering Structures 80, 339-349.

[42] Seif, M. and Schafer, B.W. (2010). Local buckling of structural steel shapes. Jounral of Constructional Steel Research 66 (10), 1232-1247.

[43] Li, Z. and Schafer, B.W. (2010). Buckling analysis of cold-formed steel members with general boundary conditions using CUFSM: conventional and constrained finite strip methods. Proceedings of the 20th International Speciality Conference on Cold-Formed Steel Structures, St. Louis, MO. November 2010.

[44] Bambach, M.R., Rasmussen, K.J.R. and Ungureanu, V. (2007). Inelastic behaviour and design of slender I-sections in minor axis bending. Journal of Constructional Steel Research 63 (1), 1-12.

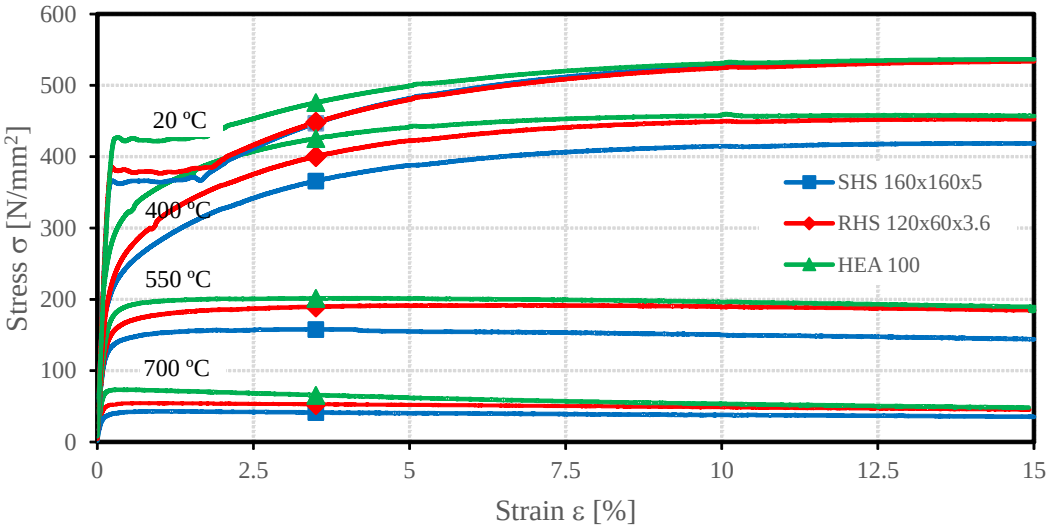

Fig.1: Tensile material response for Series 4, 6 and 8 at ambient and elevated temperatures.

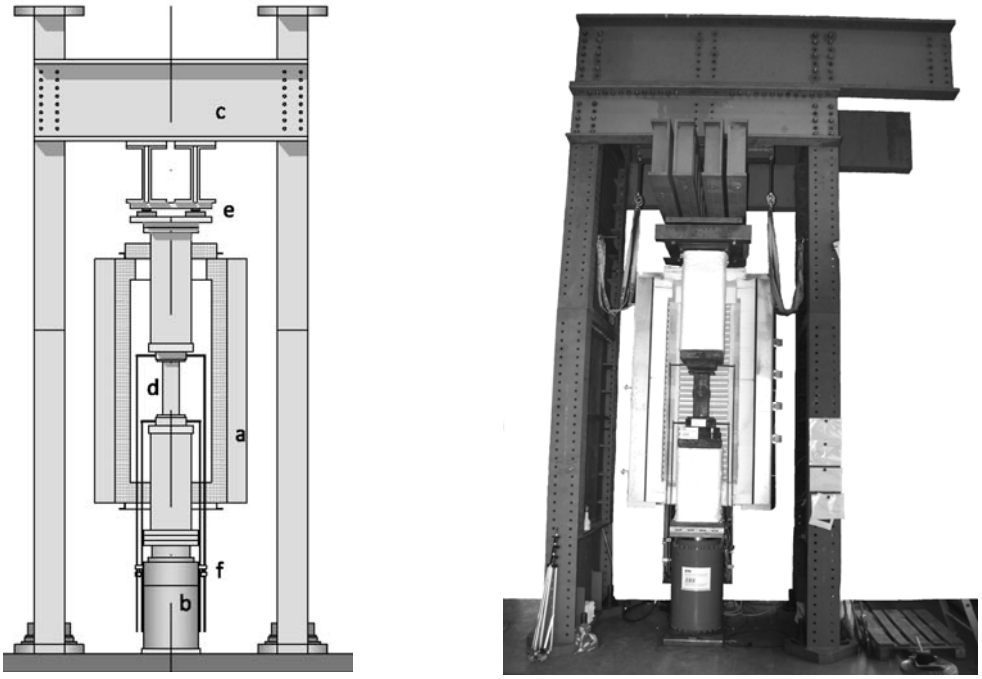

Fig. 2. Test setup for the stub column tests.

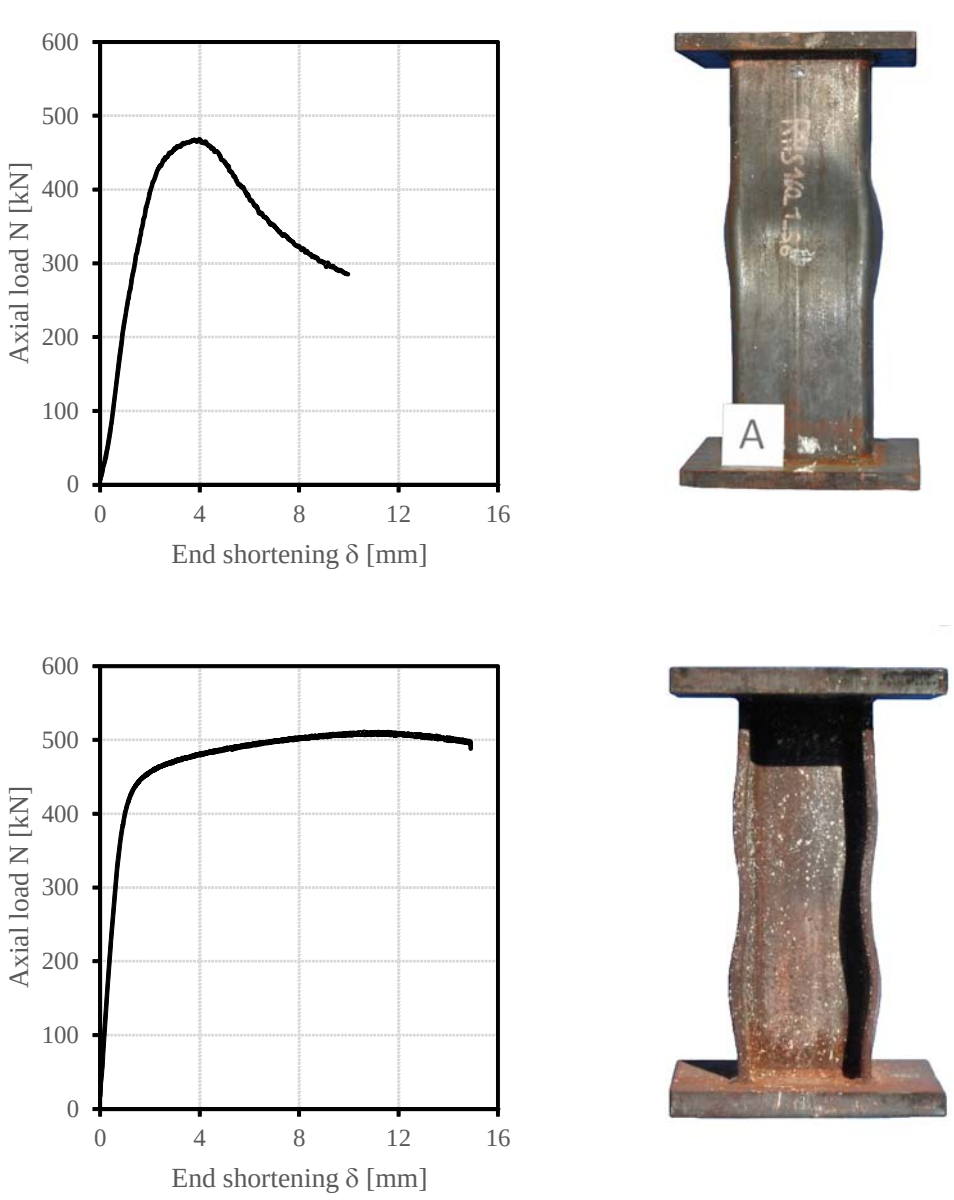

Fig. 3: Load-end shortening curve (left) and corresponding failure mode (right) for SHS 160×160×5 (top) and HEA 100 (bottom) stub column specimen at 550˚C.

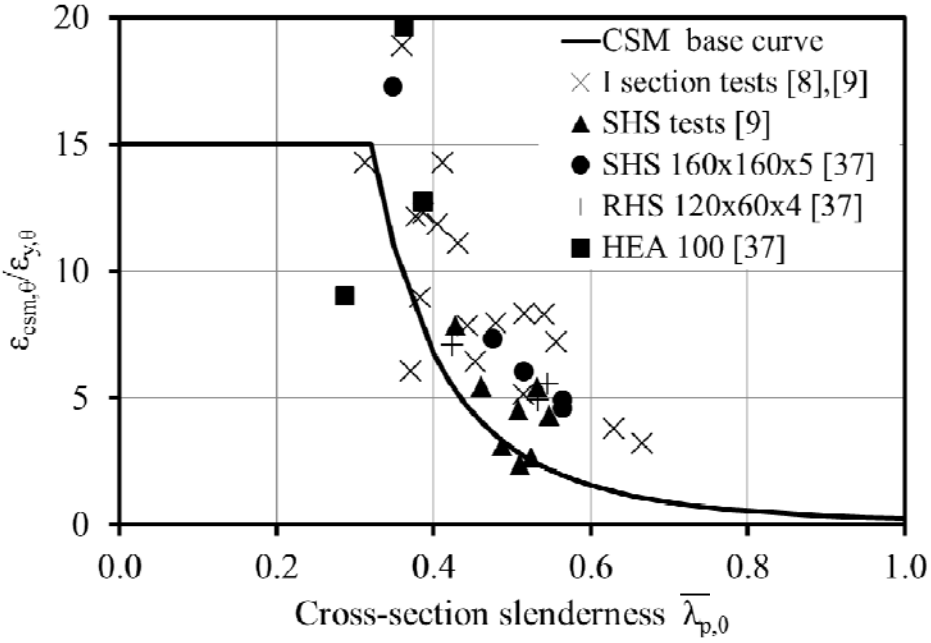

Fig. 4: Relationship between deformation capacity and slenderness, with data grouped by specimen type.

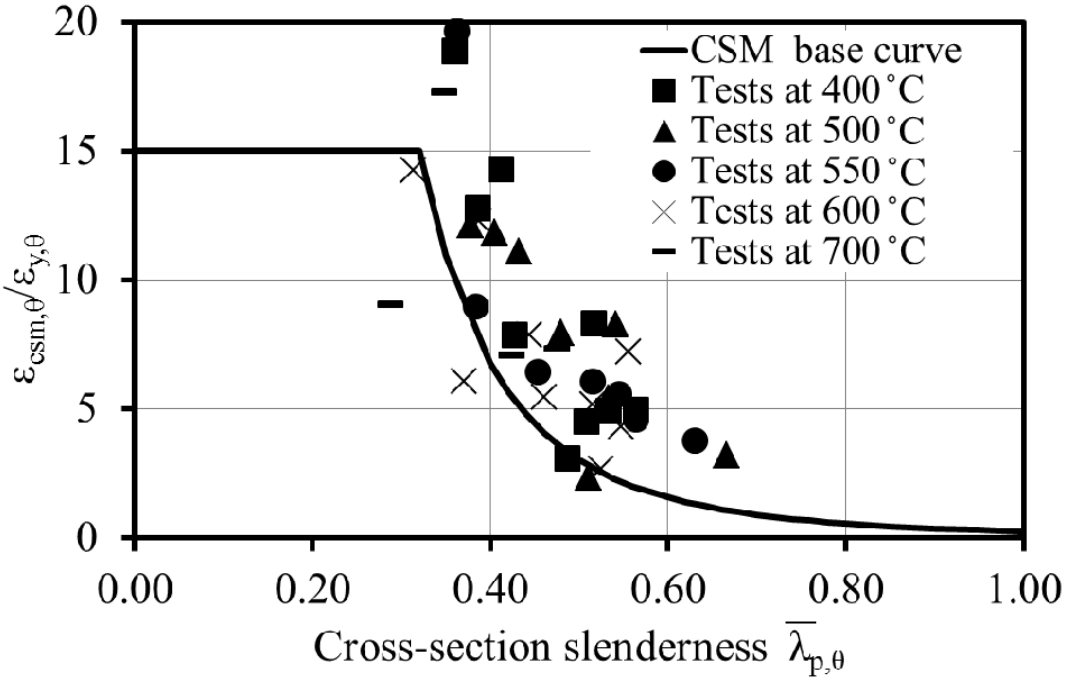

Fig. 5: Relationship between deformation capacity and slenderness, with data grouped by temperature.

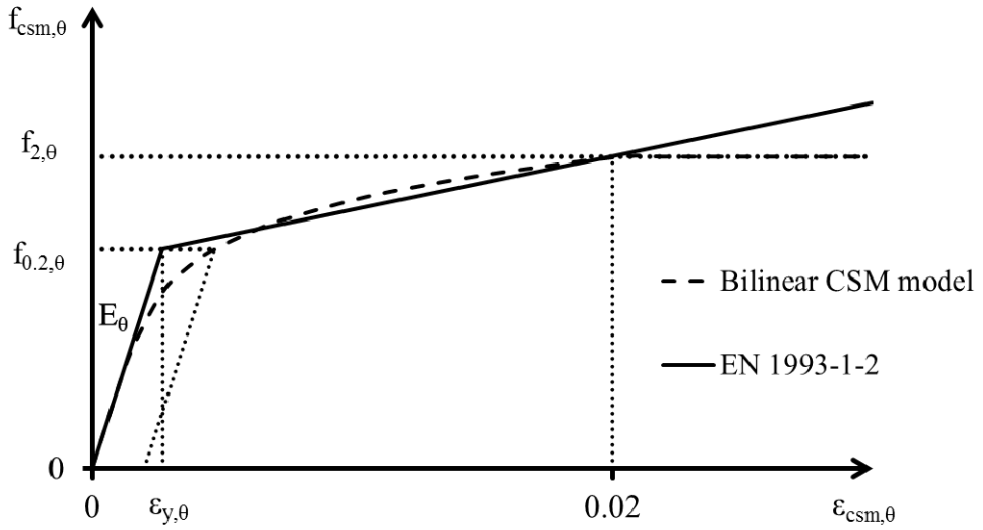

Fig. 6: Adopted bilinear CSM material model and EN1993-1-2 material model.

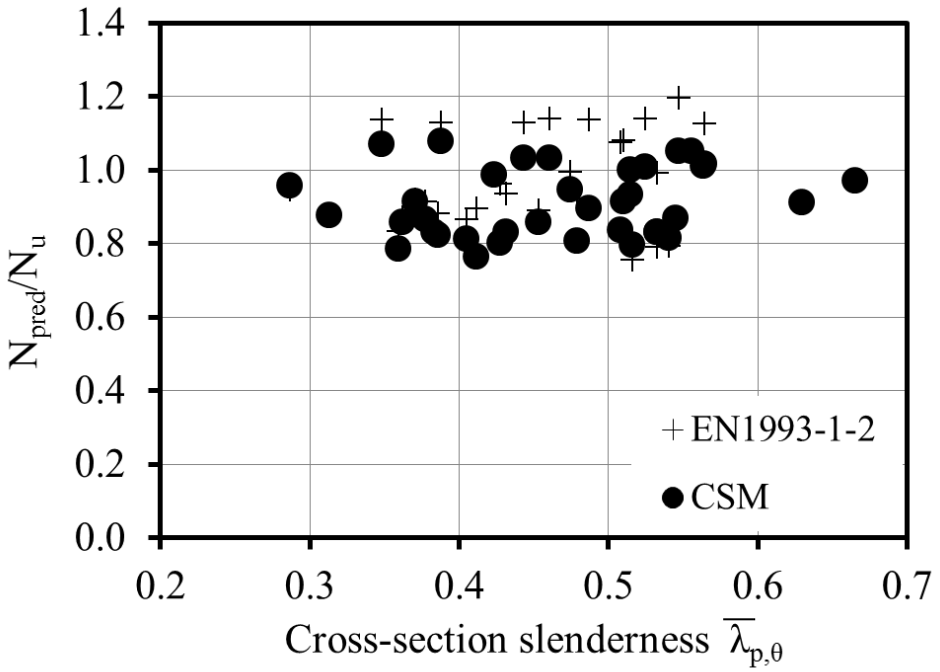

Fig. 7: Assessment of the CSM and EN 1993-1-2 design method based on isothermal stub column tests.

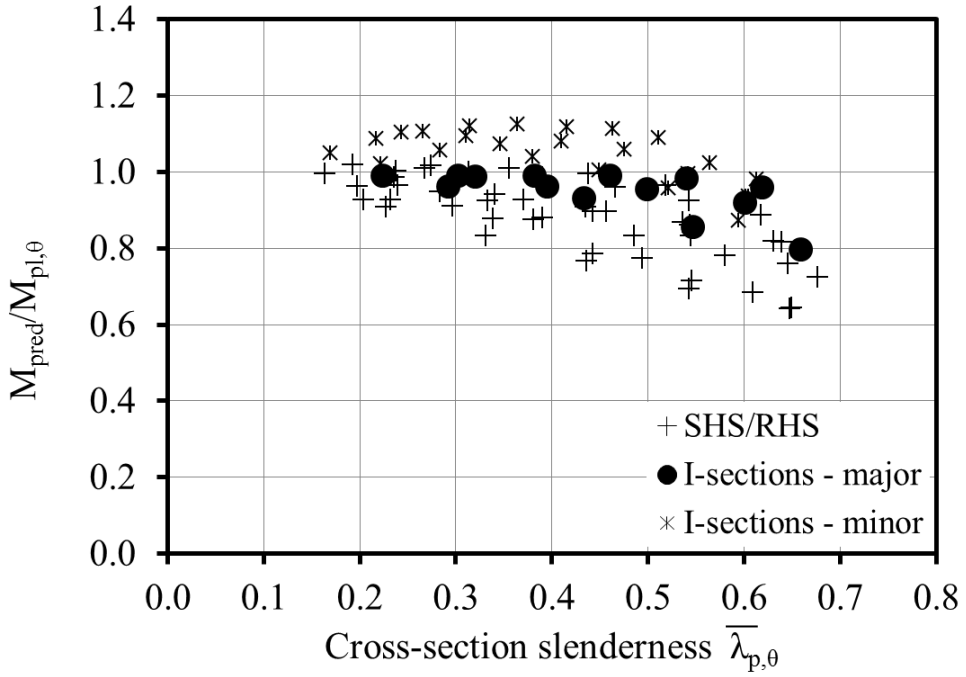

Fig. 8: Numerical moment resistances normalized by the respective plastic moment resistances with data grouped by cross-section type.

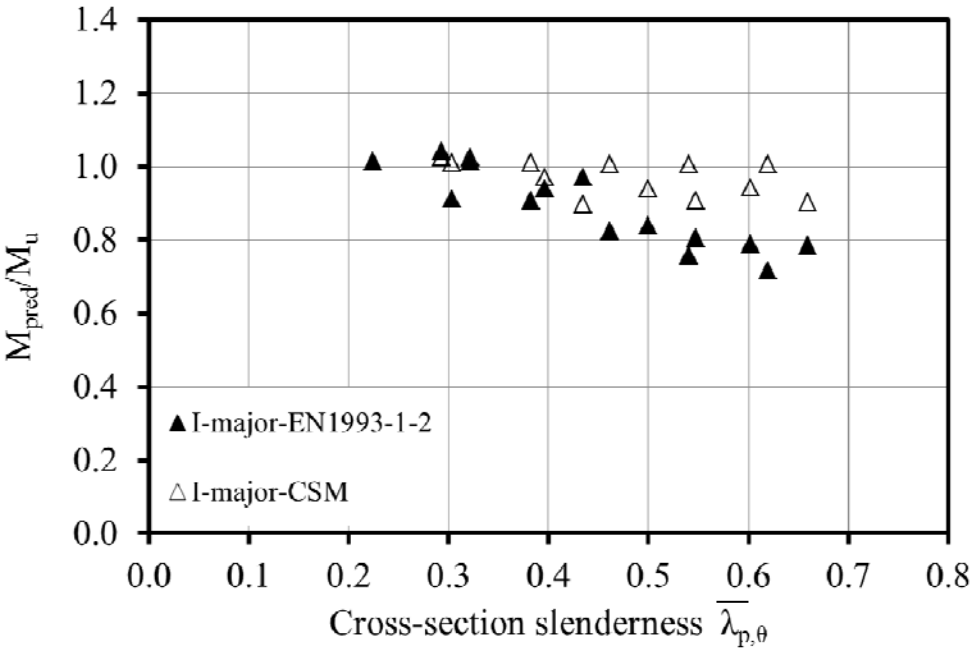

Fig. 9: Comparison of the CSM and EN 1993-1-2 for I-sections under major axis bending

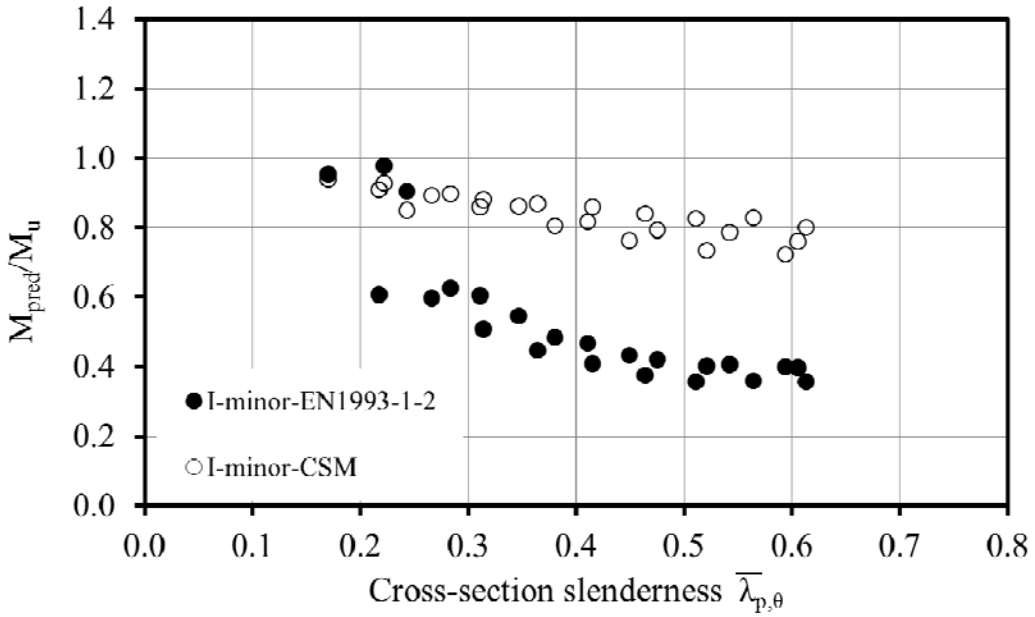

Fig. 10: Comparison of the CSM and EN 1993-1-2 for I-sections under minor axis bending

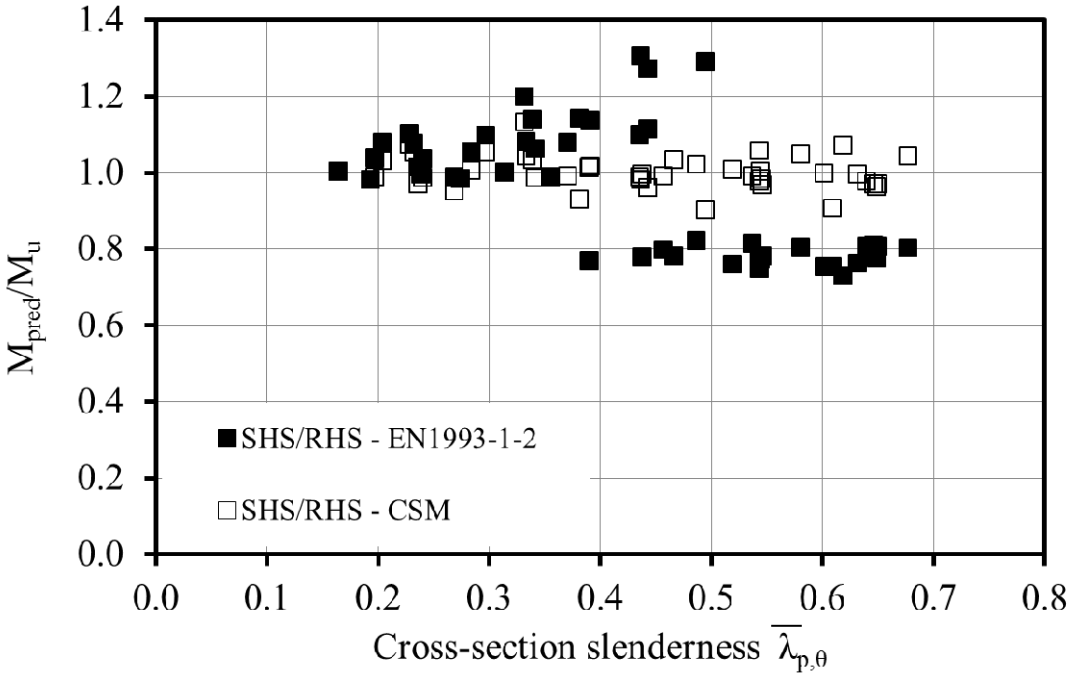

Fig. 11: Comparison of the CSM and EN 1993-1-2 for SHS and RHS

Table 1: Collated isothermal stub column tests

Source	Section type	Material grade	Temperatures considered	No. of stub column tests reported	Class at RT
Yang et al. 2006 [7]	welded I-sections	ASTM A572 Gr. 50	RT, 300˚C, 400˚C, 450˚C, 500˚C, 550˚C, 600˚C	7	3
Yang and Hsu 2009 [9]	welded I-sections	JIS SN490	RT, 500˚C, 550˚C, 600˚C	12	1-3
Yang et al. 2005 [10]	welded I-sections and SHS	Fire resistant steel	RT, 400˚C, 500˚C, 600˚C	23	1-3

[1]RT=room temperature

Table 2: Additional stub column test results [37]

Specimen	Test Series	H (mm)	B (mm)	t_w (mm)	t_f (mm)	L (mm)	T (ºC)	Strain rate (%/min)	N_u (kN)	δ_u (mm)
SHS160_Stub_400C		160.2	161.5	5.4	5.4	480	400	0.1	795	4.2
SHS160_Stub_550C		160.3	161.6	5.4	5.4	480	550	0.1	468	4.0
SHS160_Stub_550Cs	Series 4	160.4	161.2	5.4	5.4	480	550	0.02	403	4.3
SHS160_Stub_700C		160.5	161.2	5.4	5.4	480	700	0.1	138	4.4
SHS160_Stub_700Cs		160.6	160.9	5.4	5.4	480	700	0.02	88	5.3
RHS120_Stub_400C		119.4	60.5	3.9	3.9	360	400	0.1	408	3.4
RHS120_Stub_550C	Series 6	119.3	60.6	3.9	3.9	360	550	0.1	257	3.9
RHS120_Stub_700C		119.4	60.5	3.9	3.9	360	700	0.1	74	3.2
HEA100_Stub_400C		98.9	101.4	5.5	8.1	300	400	0.1	996	8.0
HEA100_Stub_550C	Series 8	98.8	101.5	5.5	8.1	300	550	0.1	511	10.6
HEA100_Stub_700C		98.9	101.4	5.5	8.1	300	700	0.1	162	3.5

Table 3: Assessment of EN 1993-1-2 and CSM based on isothermal stub column tests

Source	N_{EC3}/N_u		N_{csm}/N_u	
	Mean	COV	Mean	COV
[7]	0.88	0.03	0.88	0.06
[10]	1.01	0.14	0.90	0.12
[37]	0.98	0.19	0.94	0.09
All	0.97	0.15	0.91	0.10

Table 4: Key parameters of the FE parametric study [39]

Cross-section outer dimensions	Axis of bending	Temperatures	$\bar{\lambda}_{p,20\,°C}$ range	No. of specimens modelled	No. of utilized results
SHS 160×160	minor	20 ˚C, 400 ˚C, 550 ˚C, 700 ˚C	0.27-1.62	44	16
RHS 120×60	major		0.28-1.66	44	15
RHS 120×60	minor		0.28-1.66	44	18
I 100×100	major		0.32-1.91	44	14
I 100×100	minor		0.32-1.91	44	23

Table 5: Assessment of EN 1993-1-2 and CSM based on FE parametric study [39]

Cross-section - axis of bending	M_{EC3}/M_u		M_{csm}/M_u	
	Mean	COV	Mean	COV
I-section - major	0.88	0.12	0.97	0.05
I-section - minor	0.52	0.36	0.83	0.07
SHS	0.96	0.17	0.98	0.03
RHS - major	0.95	0.18	0.96	0.05
RHS - minor	0.93	0.21	1.01	0.03
HEA (both axes)	0.66	0.36	0.88	0.10
RHS and SHS (both axes)	0.95	0.19	0.99	0.04
All	0.82	0.30	0.94	0.09